

CrossMark  
click for updatesCite this: *RSC Adv.*, 2016, 6, 56610

# Waterborne polyurethane conjugated with novel diol chain-extender bearing cyclic phosphoramidate lateral group: synthesis, flammability and thermal degradation mechanism†

Peikun Zhang,<sup>a</sup> Zhenyu Zhang,<sup>a</sup> Haojun Fan,<sup>\*a</sup> Saiqi Tian,<sup>a</sup> Yi Chen<sup>b</sup> and Jun Yan<sup>b</sup>

A diol bearing a cyclic phosphoramidate pendant group, namely 2-(5,5-dimethyl-2-oxo-2λ<sup>5</sup>-1,3,2-dioxaphosphinan-2-ylamino)-2-methyl-propane-1,3-diol (PNMPD) was synthesized and characterized by FTIR and NMR. Subsequently, PNMPD was applied as a flame-retardant chain extender to prepare phosphorus–nitrogen containing waterborne polyurethane (PNWPU), and the influence of PNMPD on the hydrolysis, thermal and flame-retardant properties of PNWPU was investigated. The fabricated PNMPD-based PNWPU shows controllable mechanical properties and maintains the good hydrolysis-resistance property of polyurethane. Thermal stability and flammability analysis demonstrate that though the covalent conjugation of PNMPD induces a slight thermal destabilization effect, it efficiently promotes char formation in PNWPU, as a result, a 27.2% limiting oxygen index (LOI) value and a UL-94 V-0 rating can be achieved with only 12 wt% PNMPD incorporated. Compared with WPU, the peak heat release rate (PHRR), total heat release (THR), peak smoke production rate (PSPR) and total smoke release (TSR) of PNWPU-12, evaluated with cone calorimetry, are decreased by 44.7%, 39.0%, 42.9% and 36.1%, respectively. In addition, the flame retarding mechanism of PNWPU was comprehensively investigated by SEM microscopy, EDX analysis, real time FTIR and TG-FTIR, and results elucidate that these notable reductions in fire hazards are probably attributed to the formation of polyphosphoric acid-rich rugged and intumescent char in the condensed phase, which behaves as a “labyrinth effect” to effectively inhibit the transmission of heat, oxygen and volatile fragments from entering into the flame zone and shield the underlying PNWPU matrix against flame.

Received 15th March 2016  
Accepted 7th June 2016

DOI: 10.1039/c6ra06856a

www.rsc.org/advances

## 1. Introduction

Waterborne polyurethane (WPU) coatings have found extensive commercial applications in various substrates such as genuine leather, artificial leather, textile, plastics, wood and ceramics by virtue of their environment-friendly characteristics, outstanding performances and remarkable versatility.<sup>1,2</sup> Unfortunately, the intrinsically high flammability of WPU has caused plenty of fire-related events with heavy casualties and tremendous property losses over the last few years.<sup>3,4</sup> Hence, the development of flame retardant WPU is urgently required.

For a long time, the halogenated ingredients have undeniably seized a dominant position in endowing polyurethane with enhanced flame retardancy. However, the major problems encountered with these species are the generation of toxic and

potentially carcinogenic dioxins combined with corrosive fumes during combustion.<sup>5,6</sup> Consequently, tremendous research interests have been triggered in pursuit of effective halogen-free flame-retardants, among which the phosphorus and nitrogen (P–N) containing compounds are considered to be a promising alternative due to their perceived flame retardant efficiency, nontoxicity, eco-friendly and other prominent advantages.<sup>3,5–8</sup>

Generally, the P–N type flame retardants are incorporated into polyurethane by physically blending, which is recognized as the most convenient way.<sup>7–10</sup> Nevertheless, this method displays the drawbacks of considerable loading (10–30 wt%), being susceptible to leach, poor compatibility, and deterioration in mechanical properties.<sup>5,11,12</sup> In this regard, incorporation of flame retardants into polyurethane backbone or side chains *via* chemical covalent linkages so as to impart homogeneous distribution, furnish permanent flame retardancy, and maintain the mechanical strength of polyurethane have been extensively investigated.<sup>12–15</sup> Despite the aforementioned advantages, these corresponding reported P–N type waterborne polyurethanes are mainly with phosphoester-bond conjugated in the main chain, thus they are not commercially feasible owing to the easily hydrolytic phosphate ester linkages.<sup>5,16</sup> The

<sup>a</sup>Key Laboratory of Leather Chemistry and Engineering (Sichuan University), Ministry of Education, Chengdu 610065, P. R. China. E-mail: fanhaojun@163.com; Fax: +86-28-85401068; Tel: +86-28-85401068

<sup>b</sup>National Engineering Laboratory for Clean Technology of Leather Manufacture, Sichuan University, Chengdu 610065, P. R. China

† Electronic supplementary information (ESI) available. See DOI: 10.1039/c6ra06856a

hydrolyzation of organophosphate moieties will come at the expense of the scission of polyurethane backbone, which further results in the reduction of not only flame-retardant efficiency but also mechanical properties. To address this issue, one way out is to redesign reactive diol linking with P–N-containing moieties lateral chain. Unfortunately, up to now, rational design of such “ideal” reactive flame retardants with pendant phosphorus and nitrogen containing group are still scanty in the literature. In our previous work, we synthesized a pendent organophosphorus-containing chain-extender (EPPD) and conjugated it into WPU backbone to acquire flame-retardant WPU (PWPU). An LOI value of 26.6% was achieved when the EPPD content was 12 wt%, and the hydrolytic stability was improved compared to that with phosphoester bond incorporated in the main-chain structures.<sup>17</sup> Despite that, the flame-retardant efficiency of EPPD was not very high due to it contains only phosphorus, and the hydrolysis resistance of PWPU still decreased a little in comparison with neat WPU. Hence, it is necessary to develop some more efficient reactive-type phosphorus-containing derivatives with outstanding hydrolysis stability to flame retard WPU.

Previous research demonstrated that P–C and P–N bonds containing monomers and polymers have preferable resistant to hydrolysis than P–O linkages.<sup>18,19</sup> In addition, there is synergistic flame retardancy effect of phosphorus and nitrogen containing compounds on polymer matrices.<sup>13,20</sup> With this inspiration, herein, a novel halogen-free diol bearing phosphoramidate-containing moieties lateral chain, named as 2-(5,5-dimethyl-2-oxo-2λ<sup>5</sup>-1,3,2-dioxaphosphinan-2-ylamino)-2-methyl-propane-1,3-diol (PNMPD), was designed and synthesized, then it was covalently conjugated into polyurethane in the chain-extension process to obtain a series of P–N-containing fire-resistant waterborne polyurethanes (PNWPU). A complementary study on the flame-retardant characteristics and flaming mechanism of this polyurethane resin were also investigated. The substitution of a P–O bond with P–N bond is expected to improve the flame resistance of PNWPU, and simultaneously, to minimize the hydrolysis of phosphorus-containing flame retardant.

## 2. Experimental

### 2.1 Materials

Polypropylene glycol with number-average molecular weight of 2000 (PPG220) and 2,2-bis(hydroxymethyl)propionic acid (DMPA) of reagent grade were purchased from Kanto Chemical Co., Inc. (Japan) and dehydrated under high vacuum (0.8 mm<sub>Hg</sub>) at 120 °C overnight before use. Dicyclohexylmethane diisocyanate (H<sub>12</sub>MDI) of extra pure grade was commercially obtained from Wako Pure Chemical Industries, Ltd. (Japan) and was dewatered with 4 Å molecular sieves prior to synthesis. 2,2-Dimethyl-1,3-propanediol (NPG, Koei Chemical Company, Ltd., Japan), 2-amino-2-methyl-1,3-propanediol (AMPD, Tokyo Chemical Industry Co., Ltd., Japan) and stannous octoate (Sn(Oct)<sub>2</sub>, Alfa Aesar) were reagent quality and used without further purification. Phosphorus oxychloride (POCl<sub>3</sub>) was kindly received from Alfa Aesar Chemical Co., Ltd. (China) and distilled at reduced pressure before use. Other reagents and

solvents were commercially available in Sinopharm Chemical Reagent Co., Ltd. (China) and used as received.

### 2.2 Synthesis of 2-(5,5-dimethyl-2-oxo-2λ<sup>5</sup>-1,3,2-dioxaphosphinan-2-ylamino)-2-methyl-propane-1,3-diol (PNMPD)

The intermediate, 2-chloro-5,5-dimethyl-1,3,2-dioxaphosphinane-2-oxide (DOPC) was synthesized by the reaction of POCl<sub>3</sub> and NPG in the presence of chloroform, according to our previously published procedure.<sup>17</sup> FTIR (KBr)  $\nu_{\max}$  (cm<sup>-1</sup>): 2976, 2946, 2896 (–CH<sub>3</sub>/–CH<sub>2</sub>); 1304 (P=O); 1052, 1005 (P–O–C); 550 (P–Cl).

PNMPD was synthesized by nucleophilic substitution reaction of AMPD with DOPC as depicted in Scheme 1. Typically, a 250 mL four-necked round-bottom flask equipped with a thermometer, dropping funnel, mechanical stirrer and condenser connected to a tail gas absorber was charged with a mixture of AMPD (32.6 g, 0.31 mol), acetonitrile (100 mL) and triethylamine (30.4 g, 0.30 mol). The mixture was aggressively stirred at 50 °C until AMPD completely dispersed, after which the DOPC (55.4 g, 0.30 mol) dissolved in acetonitrile was carefully added dropwise to the solution within a period of 2 h. Subsequently, the reaction mixture was heated slowly up to 82 °C and kept refluxing for 6 h. After the solvent was removed by vacuum distillation, the resulting crude product was repeatedly rinsed with ethyl acetate and chloroform. Successively, the dark amber liquid, namely PNMPD, was dried for overnight to obtain a pure product having a yield of 86%. FTIR (KBr)  $\nu_{\max}$  (cm<sup>-1</sup>): 3382 (–OH and N–H); 2965, 2886 (–CH<sub>3</sub>/–CH<sub>2</sub>); 1623 (N–H); 1396 (–C(CH<sub>3</sub>)<sub>2</sub>–); 1213 (P=O); 1062 (C–O and P–O–C); 1012, 948 (P–N). <sup>1</sup>H NMR (DMSO-*d*<sub>6</sub>, 500 MHz):  $\delta$  ppm = 0.89–1.20 (m, 9H, –CH<sub>3</sub>); 3.04 (d, 4H, N–C–CH<sub>2</sub>); 3.75 (d, 4H, P–O–CH<sub>2</sub>); 4.72 (s, 2H, –OH); 7.93 (s, 1H, P–NH–). <sup>31</sup>P NMR (DMSO-*d*<sub>6</sub>):  $\delta$  ppm = –6.49.

### 2.3 Preparation of PNMPD-based waterborne polyurethane (PNWPU) dispersions

The flame-retardant waterborne polyurethanes bearing phosphorus–nitrogen moieties lateral chain were synthesized *via* prepolymer method. The sample designation and theoretical composition are tabulated in Table 1, and the polymerization process and synthesis route of PNWPU dispersions are provided in Fig. S1.† Taking PNWPU-6 for example, 30 g PPG220, 22 g H<sub>12</sub>MDI and 2.9 g DMPA were charged into a 250 mL four-necked round-bottom flask equipped with mechanical stirrer, thermometer, nitrogen inlet and condenser, and allowed to react at 80 °C for approximately 3 h in the presence of Sn(Oct)<sub>2</sub> as catalyst. Afterwards, 3.65 g PNMPD and 1.5 g NPG that dissolved in 20 mL butanone (MEK) were added to the beaker with moderate stirring and chain extended until the theoretical



Scheme 1 Synthetic route of PNMPD.

Table 1 Sample designation, composition, particle size and viscosity of PNWPU dispersions

Sample <sup>a</sup>	Theoretical composition (g)					TEA	H <sub>2</sub> O	HS <sup>b</sup> (wt%)	DMPA (wt%)	Particle size (nm)
	H <sub>12</sub> MDI	PPG220	DMPA	NPG	PNMPD					
WPU	22	30	2.9	3.0	0	2.2	108	48.19	5.01	89.78
PNWPU-3	22	30	2.9	2.25	1.82	2.2	110	49.13	4.92	91.91
PNWPU-6	22	30	2.9	1.5	3.65	2.2	112	50.04	4.83	93.65
PNWPU-9	22	30	2.9	0.75	5.47	2.2	114	50.92	4.75	117.1
PNWPU-12	22	30	2.9	0	7.3	2.2	116	51.77	4.66	137.8

<sup>a</sup> Samples here were designated as PNWPU-*x*, wherein *x* manifested the PNMPD concentration by weight of solid content in PNWPU. <sup>b</sup> Hard segment content = [mass (H<sub>12</sub>MDI + DMPA + NPG + PNMPD)]/[mass (PPG220 + H<sub>12</sub>MDI + DMPA + NPG + PNMPD)].

-NCO value was reached, which was monitored intermittently with the standard dibutylamine titration method (ASTM D 1638). Occasionally, MEK was added to adjust the viscosity of the prepolymer. After cooling the system to 50 °C, the carboxylic groups of DMPA were neutralized with 2.2 g TEA for 15 min, and then the reaction mixture was dispersed by deionized water under vigorous stirring. Finally, the solvent was removed by vacuum distillation to obtain the transparent PNWPU emulsion, in which the solid content was about 35 wt%.

#### 2.4 Characterizations and measurements

Fourier transform infrared spectroscopy (FTIR) of DOPC, PNMPD, WPU and PNWPU was captured from a Nicolet IS10 FTIR spectrometer (Nicolet Instrument Company, USA) using KBr pellets over the wavenumber range from 4000 to 400 cm<sup>-1</sup> at a resolution of 4 cm<sup>-1</sup>.

Nuclear magnetic resonance (<sup>1</sup>H NMR and <sup>31</sup>P NMR) spectra were recorded on a Bruker DRX500 MHz spectrometer (BRUKER Component, Switzerland) operating at a probe temperature of 25 °C with deuterated dimethyl sulfoxide (DMSO-*d*<sub>6</sub>) as solvent, tetramethylsilane (TMS) as the internal reference and H<sub>3</sub>PO<sub>4</sub> (85%) as the external standard.

Particle sizes of the PNWPU dispersions were determined using a Malvern Model Zeta-sizer ZEN3600 light scattering ultrafine particle analyzer at 25 °C.

Thermogravimetric analysis (TGA) was performed with a NETZSCH TA Instruments High Resolution TG 209F1 thermal analyzer under N<sub>2</sub> atmosphere from 50 to 650 °C at a scanning rate of 10 °C min<sup>-1</sup>, where the dynamic nitrogen flow was kept constant at 20 mL min<sup>-1</sup>.

The limiting oxygen index (LOI) was evaluated with a HC-2C oxygen index analyzer instrument (Jiangning Analysis Instrument Co., China) according to ASTM D 2863-2009 standard, in which the size of each sample was 127 × 10 × 3 mm<sup>3</sup> (length × width × thickness) and the average values of five replicated experiments were reported.

The UL-94 vertical burning level was conducted by a CZF-II instrument (Jiangning, China) in terms of ASTM D 3801 standard with samples fixed vertically *ca.* 300 mm above a cotton layer, of which the specimen dimension was 130 × 12.7 × 3 mm<sup>3</sup> (length × width × thickness). All specimens were repeated in quintuple.

The flammability characteristics of PNWPU films were evaluated with a cone calorimeter device (Fire Testing Technology, UK) in accordance with the procedures in ISO5660. The samples with a gauge size of 100 × 100 × 2 mm<sup>3</sup> (length × width × thickness) were wrapped in an aluminum foil and exposed horizontally at an external heat flux of 35 kW m<sup>-2</sup>.

The morphologies of char residues obtained from the burned PNWPU samples were determined by a Hitachi S-4700 scanning electron microscope (SEM) (Hitachi, Japan) at an accelerating voltage of 5 kV with an energy-dispersive X-ray (EDX) analyzer, and the surfaces were made electrically conductive by gold-sputtered before observation.

Real-time Fourier transform infrared spectra (RT-FTIR) were acquired on a Nicolet MAGNA-IR 750 FT-IR spectrophotometer having a ventilated oven with a heating device. About 10 mg of samples were ground with KBr powders and heated from ambient temperature to 600 °C, meanwhile, the dynamic FTIR was tested over the wavenumber range of 4000 to 400 cm<sup>-1</sup>.

TG-FTIR analysis was carried out on a TG 209 F1 apparatus (NETZSCH, Germany) coupled with a Nicolet IS10 FTIR spectrometer (Nicolet Instrument Company, USA). The samples (about 5 mg) were put in an alumina crucible and heated at a raised rate of 10 °C min<sup>-1</sup> in the temperature range from 40 to 650 °C under nitrogen atmosphere.

To evaluate the hydrolysis resistant ability of PNWPU, the controlled hydrolysis condition was set as follows: under an air circulating oven with a constant-temperature at 60 °C, PNWPU dispersions were incubated for 7 days. Then the treated solutions were casted on polytetrafluoroethylene plates to prepare polyurethane films. Here hydrolytic resistance was evaluated by the retention ratio of tensile properties after controlled hydrolysis. The mechanical properties of PNPWU films were measured according to ASTM D 638 standard: the dumb-bell shaped films with dimension of 50 × 10 mm<sup>2</sup> (length × width) were done in a UTM 6203 universal testing machine (Shenzhen SANS Test Machine Co. Ltd., China) with a cross-head speed of 10 mm min<sup>-1</sup> at ambient temperature.

## 3. Results and discussion

### 3.1 Characterization of PNMPD and PNWPU

Fig. 1 depicts the FTIR spectra of DOPC, PNMPD, WPU and PNWPU. The typical absorption peaks for DOPC include 2976

$\text{cm}^{-1}$ ,  $2946 \text{ cm}^{-1}$  and  $2896 \text{ cm}^{-1}$  ( $-\text{CH}_3/-\text{CH}_2$ ),  $1304 \text{ cm}^{-1}$  ( $\text{P}=\text{O}$ ),  $1052 \text{ cm}^{-1}$  and  $1005 \text{ cm}^{-1}$  ( $\text{P}-\text{O}-\text{C}$ ),  $550 \text{ cm}^{-1}$  ( $\text{P}-\text{Cl}$ ), which is in good correlation with the prior literature.<sup>21</sup> Compared with DOPC, several characteristic absorption bands for PNMPD appear at  $3382 \text{ cm}^{-1}$ ,  $1623 \text{ cm}^{-1}$ ,  $1213 \text{ cm}^{-1}$  and  $1012 \text{ cm}^{-1}$ , which correspond to the stretching vibration of  $-\text{OH}$  and  $\text{N}-\text{H}$ ,  $\text{N}-\text{H}$  deformation,  $\text{P}=\text{O}$  stretching vibration and  $\text{P}-\text{N}$  bond, respectively. Notably, the synthesis of PNMPD was carried out by substitution reaction, during which the chlorine in DOPC was consumed by the reaction with amino group in AMPD, thus resulting in the disappearance of  $\text{P}-\text{Cl}$  at  $550 \text{ cm}^{-1}$ , thereby directly signifying the successful synthesis of PNMPD. The formation of PNMPD was also corroborated by  $^1\text{H}$  NMR and  $^{31}\text{P}$  NMR spectra, as presented in Fig. 2. The broad peak centered at  $4.72 \text{ ppm}$  is assigned to the protons of  $-\text{OH}$ , and the single peak at  $7.93 \text{ ppm}$  is ascribed to the secondary amine proton, while the high-field signals at  $0.89\text{--}1.20 \text{ ppm}$  are reasonably attributed to the methyl protons. More importantly, only an intensive singlet signal for phosphorus is observed at  $-6.49 \text{ ppm}$  in the  $^{31}\text{P}$  NMR spectrum. Taken together, these results prove that the PNMPD is fabricated successfully.

To validate the feasible covalently conjugation between PNMPD and NCO-terminated prepolymer, the chemical structure of WPU together with PNWPU was systematically characterized by FTIR,  $^1\text{H}$  and  $^{31}\text{P}$  NMR spectroscopy. In the FTIR spectrum of WPU displayed in Fig. 1, the representative absorption peaks appearing at  $3345 \text{ cm}^{-1}$  (urethane  $\text{N}-\text{H}$  stretching),  $2970 \text{ cm}^{-1}$ ,  $2925 \text{ cm}^{-1}$  and  $2859 \text{ cm}^{-1}$  ( $\text{C}-\text{H}$  symmetric and asymmetric stretching),  $1707 \text{ cm}^{-1}$  ( $\text{C}=\text{O}$  functional group),  $1533 \text{ cm}^{-1}$  (urethane  $\text{N}-\text{H}$  bend vibration), and  $1104 \text{ cm}^{-1}$  ( $\text{C}-\text{O}-\text{C}$ ) are detected. By comparison, in addition to the aforementioned characteristic bands corresponding to polyurethane, some new absorption peaks emerge in the FTIR spectrum of PNWPU. In detail, the presence of  $\text{N}-\text{H}$  bending band from phosphamide is clearly evident at  $1633 \text{ cm}^{-1}$ , whilst the bands at  $1305 \text{ cm}^{-1}$  and  $1013 \text{ cm}^{-1}$  are

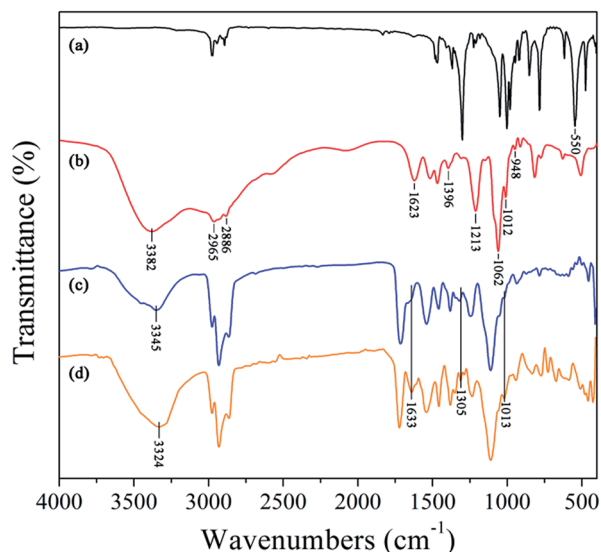


Fig. 1 FTIR spectra of DOPC (a), PNMPD (b), WPU (c) and PNWPU (d).

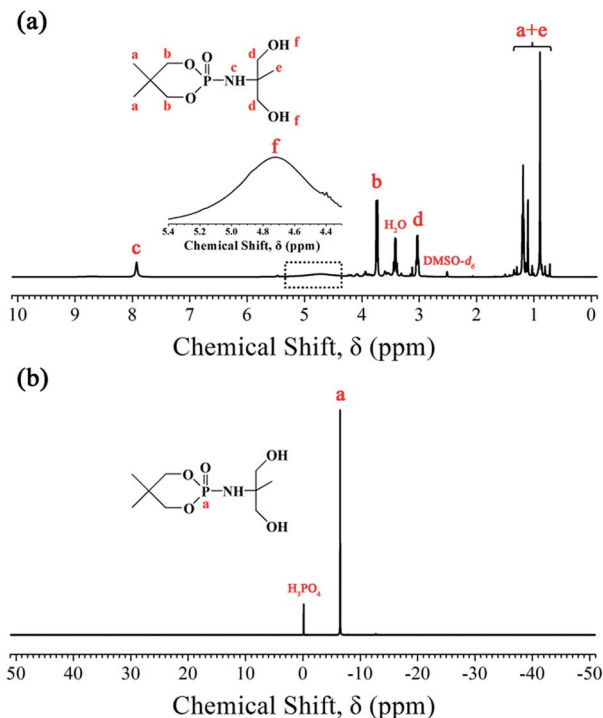


Fig. 2  $^1\text{H}$  NMR (a) and  $^{31}\text{P}$  NMR (b) spectra of PNMPD.

attributable to the vibration of  $\text{P}=\text{O}$  and  $\text{P}-\text{N}$ , respectively. Unfortunately, as a consequence of band overlapping in the  $1000\text{--}1200 \text{ cm}^{-1}$  region, the stretching vibration modes of  $\text{P}-\text{O}-\text{C}$  cannot be revealed distinctly. However, the absorption intensity of  $\text{N}-\text{H}$  stretching vibration for PNWPU is visibly increased and shows a slightly redshift to downward wavenumber centered at  $3324 \text{ cm}^{-1}$ , presumably owing to the extra hydrogen bonding participated by urethane carbonyl groups and  $\text{N}-\text{H}$  from phosphamide.<sup>22</sup> This explication is supported by the trifling downfield of secondary amine proton from  $6.98 \text{ ppm}$  to around  $7.01 \text{ ppm}$  with multiplet resonance signals in consequence of the enhanced deshielding effects,<sup>23</sup> as revealed by  $^1\text{H}$  NMR spectrum in Fig. 3. Besides that, a new chemical shift at  $3.01 \text{ ppm}$  as the assignment for methylene protons adjacent to urethane linkage is determined, and the peak at  $1.17 \text{ ppm}$  is associated with the methyl protons in PNMPD. Of critical importance, the  $^{31}\text{P}$  NMR spectrum exhibits only a single peak at  $-5.14 \text{ ppm}$ , corresponding to the phosphorus proton originating from the pendent group of PNMPD segment in polyurethane. Associated with the FTIR results previously described, it can be concluded that the PNMPD diols are intimately and permanently tethered on PNWPU with phosphorus-nitrogen moieties in lateral chain.

### 3.2 Hydrolytic resistance of PNWPU

The main concern for organophosphorus-containing water-borne polyurethane is that phosphoester groups tend to hydrolyze in emulsion during transport or storage, which leads to the decrease of molecular weight and mechanical properties, thus limits their use in many practical applications.<sup>16,24</sup> Here the tensile strength and elongation at break of PNWPU films along

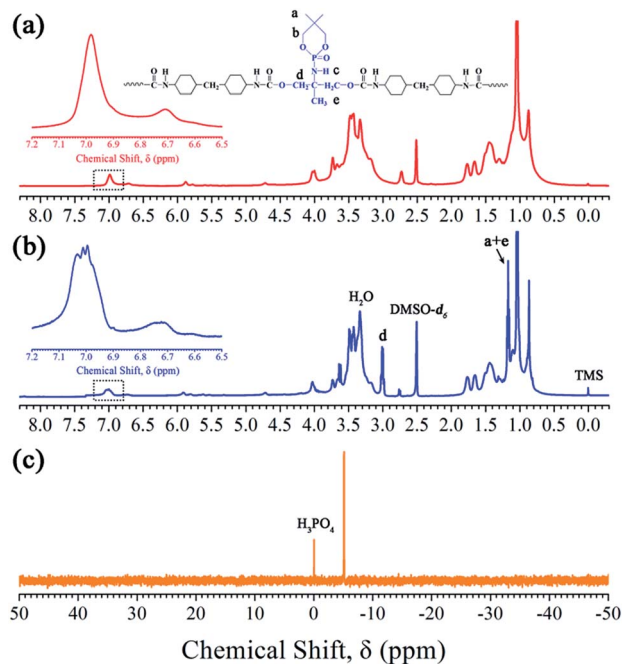


Fig. 3  $^1\text{H}$  NMR spectra of WPU (a) and PNWPU (b), and  $^{31}\text{P}$  NMR spectra of PNWPU (c).

with the retention ratio of mechanical properties after hydrolytic treatment at 60 °C for a week are given in Table 2. Qualitatively, with the conjugation of PNMPD flame retardant, the ultimate tensile strength drops systematically from 15.0 MPa for WPU to 8.2 MPa for PNWPU-12. However, the broken elongation increases firstly and then decreases. Generally, the interconnectivity and phase separation of the hard segment are two main influential factors that determine the mechanical strength of the two-phase polyurethane.<sup>25</sup> Structurally speaking, the methyl and the bulky cyclothiophosphoramidate are anchoring in the side-chain of PNMPD by means of special molecular design. When conjugated into PNWPU, the steric hindrance effects induced by these lateral groups in PNMPD are capable of disrupting the crystallization of hard segments and encumbering the intermolecular reaction of polyurethane chains, thus facilitates the slipping of macromolecular chains.<sup>26</sup> Meanwhile, the organophosphate flame retardant has an internal plasticization effect on polyurethane matrix, which leads to soft resins and the decrease of tensile strength. On the other hand, the appreciable reduce in ductility for PNWPU-12 may be

attributable to the concentrated structural defects with increasing PNMPD content.

As listed in Table 2, WPU displays a favourable hydrolysis performance, which is reflected by the high retention ratio of more than 93% in mechanical properties. Further, it is interesting to note that the retention rate for all PNWPU films is basically equivalent to that of WPU, indicating that the anchoring of phosphamide in the dangling chains of polyurethane does not deteriorate the hydrolysis-resistance property. Another evidence for the excellent hydrolysis stability is illustrated by the trifling changes of flame retardancy after controlled hydrolysis shown in Table 4. Actually, during the hydrolyzation process of phosphorus-containing waterborne polyurethane dispersions, the predominant reaction is the cleavage of phosphate ester linkages, followed by urethane bonds.<sup>27</sup> Hence, without exaggeration, the hydrolytic resistance of the PNWPU is essentially determined by the phosphamide groups. For our designed PNMPD monomer, one of the easily hydrolyzable P–O linkage is well-substituted by P–N bond, which shows preferable resistant to hydrolysis.<sup>19</sup> On the other hand, in the PNWPU dispersions, the phosphoramidate is just as a “core” that surrounded by the “shells” of sixth position’s hydrophobic methyl groups in NPG and dioxaphosphorinane of PNMPD, conforming to the Newman’s “rule of six”.<sup>28</sup> Accordingly, these moisture-sensitive moieties are resistant to hydrolyse, which endows the pendant phosphamide groups bearing PNWPU far better hydrolysis stability than previously reported phosphate-based polymers.<sup>17,19</sup>

### 3.3 Thermal stability of PNMPD and PNWPU

The thermal stability and thermal decomposition behavior of PNMPD and PNWPU were investigated by TGA in nitrogen atmosphere. Typical TGA and DTG thermograms for PNMPD and PNWPU are plotted in Fig. 4, and the detailed thermal decomposition data are enumerated in Table 3.

Clearly, PNMPD decomposes in three main stages as shown in Fig. 4, of which the maximum degradation temperature ( $T_{\text{max}}$ ) are around 253.1 °C, 309.4 °C and 487.2 °C, respectively. Furthermore, the 5 wt% weight loss temperature ( $T_{\text{d5\%}}$ ) of PNMPD is 211.7 °C, while the char residues at 650 °C is 16.7 wt%, demonstrating that PNMPD is an efficient char-forming agent.

Fig. 4 shows that both WPU and PNWPU samples display a three main stage degradation processes. According to previous studies, the first and second decomposition occurred around 200–350 °C is related to the cleavages of the urethane

Table 2 Mechanical properties of WPU and PNWPU films before and after hydrolysis

Sample	Tensile strength (MPa)			Elongation at break (%)		
	Before hydrolysis	After hydrolysis	Retention ratio (%)	Before hydrolysis	After hydrolysis	Retention ratio (%)
WPU	15.0 ± 0.3	14.1 ± 0.3	94.0	385.6 ± 13.2	359.0 ± 10.6	93.1
PNWPU-3	12.1 ± 0.4	11.4 ± 0.3	94.2	432.3 ± 15.8	399.1 ± 9.7	92.3
PNWPU-6	11.1 ± 0.2	10.4 ± 0.4	93.7	488.9 ± 9.4	448.9 ± 14.5	91.8
PNWPU-9	10.2 ± 0.3	9.5 ± 0.2	93.1	499.4 ± 20.3	463.5 ± 12.1	92.6
PNWPU-12	8.2 ± 0.2	7.7 ± 0.3	93.9	443.4 ± 8.2	409.3 ± 7.4	92.3

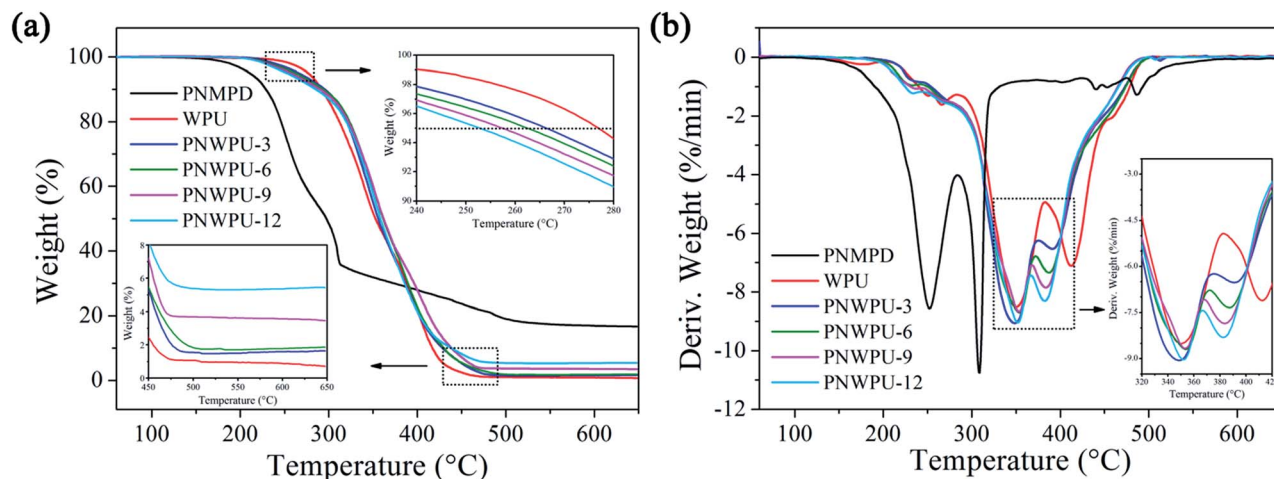


Fig. 4 TGA (a) and DTG (b) curves of PNMPD, WPU and PNWPU under nitrogen.

Table 3 TGA data for PNMPD, WPU and PNWPU

Sample	$T_{d5\%}^a$ (°C)	$T_{max1}^b$ (°C)	$T_{max2}^b$ (°C)	$T_{max3}^b$ (°C)	$Y_c^c$ (%)
PNMPD	211.7	253.1	309.4	487.2	16.7
WPU	276.9	265.5	349.7	411.8	0.71
PNWPU-3	265.9	234.7	348.2	390.6	1.63
PNWPU-6	261.9	232.3	353.3	386.5	1.86
PNWPU-9	256.6	237.6	352.4	382.9	3.46
PNWPU-12	252.8	233.9	351.9	382.4	5.44

<sup>a</sup>  $T_{d5\%}$  is defined as the temperature at which the samples undergo 5 wt% weight loss. <sup>b</sup>  $T_{max}$  is defined as the temperature at which the decomposition rate of the samples reach a maximum. <sup>c</sup> Char yield at 650 °C.

bonds in hard segments, while the third step at 350–480 °C corresponds to the scission of soft segments.<sup>29,30</sup> For WPU film, the  $T_{d5\%}$  is around 276.9 °C with the  $T_{max}$  at 265.5 °C, 339.9 °C and 402.2 °C, respectively, and its residual char at 650 °C is 0.71 wt%, which reflects that WPU itself has a negligible char-forming ability. Compared with WPU, the  $T_{d5\%}$  and  $T_{max}$  of all PNWPU samples show a tendency of decrease. This may be correlated with the relatively inferior thermal stable O=P-O and P-O-C bond in PNMPD segment.<sup>31,32</sup> However, the degradation of phosphoester bond can promote the formation of polyphosphoric acid or its derivatives, which will catalyze the decomposition of polyurethane to produce additional thermally stable phosphorous-rich carbonaceous layers at elevated temperature.<sup>9,33</sup> Consequently, the residue percentage at 650 °C is significantly increased from 0.71 wt% for WPU to 5.44 wt% for PNWPU-12. The high char yield is suggested to block the volatilization of combustible gases and inhibit the exothermicity of pyrolysis reaction according to the solid phase mechanism of such phosphoramidate-based flame retardant, thus bestowing polyurethane with high flame retardancy.<sup>10,11,34</sup>

### 3.4 Flame retardancy of PNWPU

The LOI and UL-94 vertical burning tests were used as a quantitative analytical method to evaluate the flammability of

PNWPU, and the data are summarized in Table 4. Briefly, the LOI value increases monotonically from 18.5% for WPU to 27.2% for PNWPU-12, proving the enhanced flame retardancy effect of PNMPD in polyurethane. Direct visual observation reveals that when subjected to the butane flame at an oxygen concentration of 21.0 vol%, the WPU ignites instantly with vigorous flame propagation, and molten droplet with fire is observable. This melt dripping phenomenon is undesirable due to its propensity to spread fire to neighboring ignitable materials, thereby increasing the potential fire hazard. Furthermore, as a consequence of highly flammable characteristic, the WPU specimen burns readily accompanied with serious bending deformation till extinguishes by violent melt-dripping behaviors. The burning process changes significantly with the anchoring of PNMPD. At an oxygen concentration of 22.4 vol%, when PNWPU-6 sample is ignited, the flame gradually becomes small and then extinguishes with apparent melt-dripping. While for PNWPU-12, following ignition, the flame propagates slowly with only dim and lethargic blaze burns the testing bar at the oxygen concentration of 27.2 vol%, and finally self-extinguishes without aggressive molten dripping. Moreover, PNMPD imparts waterborne polyurethane with better fire resistance than our previously synthesized pendant phosphorus-containing chain extender at the same loading of flame retardant. For example, the LOI value increases from 26.6% to 27.2% when conjugated with 12 wt% flame retardant.<sup>17</sup> This declares that the pendant phosphoramidate-containing PNMPD is capable of suppressing the molten drops to induce carbonization efficiently and there is a synergistic effect in P and N element, which would allot PNWPU with improved flame retardancy. The virtually nonflammable feature of PNWPU is also affirmed by the vertical burning test. That is, with 12 wt% PNMPD conjugated, the corresponding polyurethane can easily pass UL-94 V-0 rating whilst WPU shows no classification. In more detail, the WPU test specimen keeps burning autogenously to the holding clamp and burns out completely with serious melt dripping after first burner flame application. Consequently, no UL-94 rating is obtained. For

Table 4 LOI and UL-94 values of WPU and PNWPU specimens

Sample	Untreated					After controlled hydrolysis				
	LOI (%)	UL-94		Drops	Rating	LOI (%)	UL-94		Drops	Rating
$t_1^a$ (s)	$t_2^b$ (s)	LOI (%)	$t_1$ (s)			$t_2$ (s)				
WPU	18.5 ± 0.1	52 ± 5	None <sup>c</sup>	Yes	Fail	18.5 ± 0.1	51 ± 6	None	Yes	Fail
PNWPU-3	19.6 ± 0.2	55 ± 4	None	Yes	Fail	19.6 ± 0.1	53 ± 4	None	Yes	Fail
PNWPU-6	22.4 ± 0.2	18 ± 3	8 ± 2	Yes	V-2	22.3 ± 0.2	19 ± 3	8 ± 3	Yes	V-2
PNWPU-9	25.3 ± 0.1	10 ± 2	6 ± 2	No	V-1	25.1 ± 0.2	10 ± 3	6 ± 2	No	V-1
PNWPU-12	27.2 ± 0.2	3 ± 1	2 ± 1	No	V-0	27.1 ± 0.1	3 ± 1	2 ± 1	No	V-0

<sup>a</sup> Time to self-extinguishing after first burner flame application. <sup>b</sup> Time to self-extinguishing after second burner flame application. <sup>c</sup> The specimens burn up to holding clamp and burn out completely after first burner flame application.

PNWPU-6, the average duration of flaming combustion after the burner flame application is 18 s and 8 s, respectively. Unfortunately, flaming drips ignite the cotton placed below samples, thus the UL-94 test rating is V-2. With further increased PNMPD concentration to 12 wt%, PNWPU-12 exhibits better fire performance and excellent anti-dripping behaviour, and a UL-94 V-0 rating is achieved.

The cone calorimeter is an efficient method to simulate a developing fire scenario for quantifying the combustion behaviors of polymers. Herein, some meaningful parameters, including heat release rate (HRR), total heat release (THR), smoke production rate (SPR), total smoke release (TSR) are

plotted in Fig. 5, and other corresponding data are recorded in Table 5. It can be observed from Fig. 5 that WPU burns rapidly after ignition with a THR and peak HRR (PHRR) of 71.5 MJ m<sup>-2</sup> and 1059 kW m<sup>-2</sup>, respectively. For PNWPUs, as the PNMPD content increases, the THR and PHRR values decrease. In detail, the PHRR of PNWPU-12 is 586 kW m<sup>-2</sup>, accounting for 55.3% of that of WPU. While the THR for PNWPU-12 shows a 39.0% reduction from 71.5 MJ m<sup>-2</sup> to 43.6 MJ m<sup>-2</sup>.

Based on the HRR curves, the fire growth rate (FIGRA) and maximum average rate of heat emission (MAHRE) are proposed to estimate the fire spread rate and burning propensity for fire development under full-scale conditions.<sup>35</sup> FIGRA is calculated

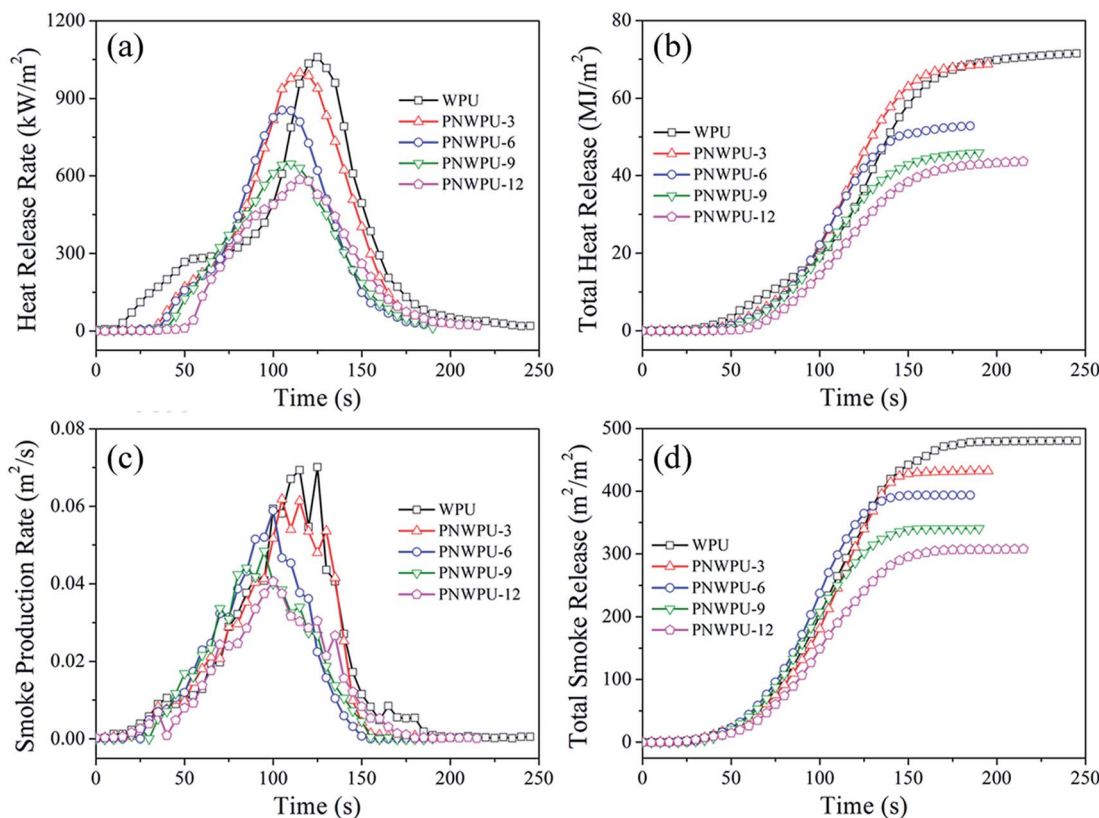


Fig. 5 HRR (a), THR (b), SPR (c) and TSR (d) versus time curves of WPU and PNWPU at an applied flux of 35 kW m<sup>-2</sup>.

Table 5 Cone calorimeter data for WPU and PNWPU films

Sample	WPU	PNWPU-3	PNWPU-6	PNWPU-9	PNWPU-12
TTI (s)	10 ± 1	19 ± 2	23 ± 2	28 ± 3	39 ± 3
PHRR (kW m <sup>-2</sup> )	1059 ± 27	998 ± 15	854 ± 13	646 ± 9	586 ± 10
TPPHRR (s)	125 ± 5	115 ± 3	105 ± 4	110 ± 5	115 ± 4
THR (MJ m <sup>-2</sup> )	71.5 ± 2.3	68.7 ± 1.7	52.8 ± 0.9	45.9 ± 1.1	43.6 ± 0.7
AHRR (kW m <sup>-2</sup> )	296 ± 11	332 ± 13	278 ± 8	235 ± 9	198 ± 6
FIGRA (kW m <sup>-2</sup> s <sup>-1</sup> )	8.5 ± 0.2	8.7 ± 0.3	8.1 ± 0.2	5.9 ± 0.1	5.1 ± 0.1
FPI (m <sup>2</sup> s kW <sup>-1</sup> )	0.009 ± 0.001	0.019 ± 0.002	0.027 ± 0.002	0.043 ± 0.003	0.067 ± 0.004
MARHE (kW m <sup>-2</sup> )	423 ± 15	414 ± 11	349 ± 10	289 ± 8	255 ± 5
AEHC (MJ kg <sup>-1</sup> )	22.9 ± 0.3	22.7 ± 0.4	23.3 ± 0.3	23.0 ± 0.2	22.4 ± 0.1
AMLR (g s <sup>-1</sup> )	0.129 ± 0.010	0.126 ± 0.009	0.107 ± 0.009	0.105 ± 0.008	0.099 ± 0.007
TSR (m <sup>2</sup> m <sup>-2</sup> )	482 ± 16	432 ± 17	393 ± 11	340 ± 12	308 ± 9
PSPR (m <sup>2</sup> s <sup>-1</sup> )	0.070 ± 0.006	0.062 ± 0.005	0.059 ± 0.005	0.048 ± 0.004	0.040 ± 0.004
Residue (%)	2.0 ± 0.2	3.5 ± 0.3	5.6 ± 0.5	11.1 ± 0.4	16.6 ± 0.6

by the ratio of PHRR and time to PHRR (TPPHRR) whereas MAHRE is derived from the cumulative heat emission divided by time.<sup>36,37</sup> The FIGRA value is 8.5 kW m<sup>-2</sup> s<sup>-1</sup> for WPU while 5.1 kW m<sup>-2</sup> s<sup>-1</sup> for PNWPU-12. The MAHRE parameter for PNWPU-12 drops by 39.7% in comparison with that of WPU, demonstrating that the conjugation of PNMPD slows the flame spread potential, which provides crucial time in a real world fire scenario for safe evacuation and other emergency measures to be taken. Besides that, fire performance index (FPI), defined as the proportion of time to ignition (TTI) to PHRR, is believed to be the best single indicator for overall fire hazard evaluation posed by polyurethane. Generally, a higher FPI value suggests the longer time to flashover, and *vice versa*.<sup>38</sup> From Table 5, it is obvious that the FPI is strikingly increased with concentrated PNMPD, further confirming an improvement of the fire safety of phosphorus- and nitrogen-containing polyurethane.

Highly dense smoke during the fire may severely reduce the visibility to slow down safe evacuation or even put residents to death directly by the toxic fumes.<sup>39</sup> Hence, smoke suppression is of vital importance. The overlay plots of the SPR and TSR are displayed in Fig. 5c and d. The TSR value for PNWPU-12 is 308 m<sup>2</sup> m<sup>-2</sup>, much lower than 482 m<sup>2</sup> m<sup>-2</sup> for WPU. Moreover, the peak smoke production release (PSPR) of PNWPU-12 is merely 0.040 m<sup>2</sup> s<sup>-1</sup>, 57% of that of WPU. Consequently, both results illustrate that the conjugation of PNMPD has a positive effect in inhibiting smoke production.

It is noteworthy that the TSR not only reflects the release of smoke hazards, but also discloses the flame retardancy mechanism. A decrease in TSR evinces that the condensed-phase flame-retardant effect plays the dominating role in PNWPU.<sup>33,40</sup> This statement is supported by the indiscernible change of average effective heat combustion (AEHC) value. That is, if a polymer exhibits flame retarding effect mainly in the gaseous phase, the combustion of the volatilized substances would be incomplete, thus resulting in the decrease of both HRR and AEHC.<sup>41,42</sup> Another evidence to further verify the above assertion can be found by the dramatically increased char residues from 2.0% for WPU to 16.6% for PNWPU-12 as revealed in Table 5, which is in accord with TGA results. On the basis of the above considerations, it might be reasonable to describe as

follow: during combustion, the phosphorus- and nitrogen-containing PNMPD facilitates the formation of consolidated carbonaceous layer, which acts as a barrier to inhibit the diffusion of flammable volatile fragments and prevent the underlying polyurethane from heat and oxygen.

### 3.5 Flame retarding mechanism

Previous studies have preliminarily validated that the residue chars is important to the flame retardancy of polyurethane. To further elucidate clearly the effects of PNMPD component on the char formation of PNWPU, the microstructures as well as chemical composition of residual chars after cone calorimeter testing were assessed by SEM and EDX spectroscopy. Fig. 6 reports some snapshots for WPU and PNWPU chars after cone calorimeter tests. As can be seen from Fig. 6a that the WPU is almost burnt out, leaving limited poor residue. For the PNWPU-

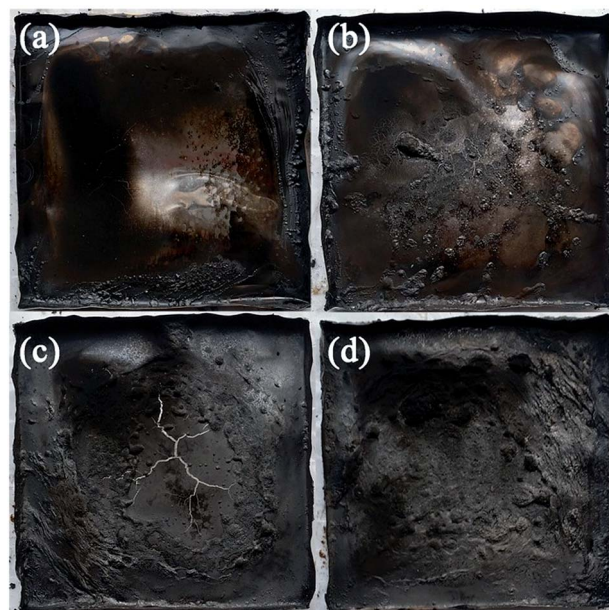


Fig. 6 Digital photographs of residues for WPU (a), PNWPU-3 (b), PNWPU-9 (c), and PNWPU-12 (d) after cone calorimeter test.

9 sample, the char is fragile and discrete. As the PNMPD increases to 12%, a swollen, dense and intact char layer is observed, which can efficiently impede both mass and heat transfer. Fig. 7 presents the SEM micrographs of the residue surfaces of WPU and PNWPU-12. The WPU char is susceptible to cracking during combustion and seems rather flattened in high magnification (Fig. 7a and b). When the combustion occurs, heat and oxygen are easily transferred through the fractured surface. By comparison, the surface of PNWPU-12 shows a more swollen and intumescent char structure with lots of irregular and discontinuous bubbles of about 100  $\mu\text{m}$  diameter. Specially, the microstructure of PNWPU-12 char consists of plenty of rugged creases (shown in Fig. 7d), as if a wrinkled “carbonaceous clothes” dressed on the unburned polyurethane matrix. Such morphology is pivotal in preventing the rapid volatilization of the inside pyrolysis products from entering into the flame zone,<sup>43</sup> consequently attributing to the improvement of flame retardancy in polyurethane.

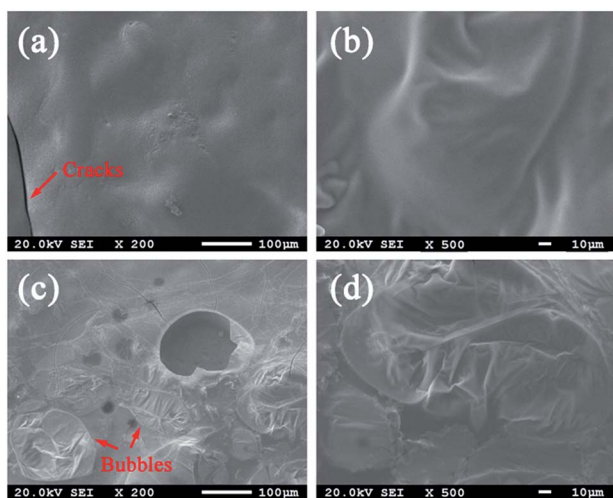


Fig. 7 SEM microphotographs of the residual chars for WPU (a and b) and PNWPU-12 (c and d) at different magnifications.

The EDX spectrum (see Fig. S2†) demonstrates that the atom percentages of oxygen and phosphorus in PNWPU-12 residues are 23.81% and 5.83%, respectively. The phosphorus content is much higher than that in PNWPU-12 film (1.47%), illustrating that the majority of phosphate derived from PNMPD remains in the condensed phase. Additionally, the molar ratio of O to P approaching 4 : 1 suggests that polyphosphoric acid or its derivative exist in the char.<sup>33</sup>

Condensed phase and gaseous phase are two important aspects that significantly contribute to comprehensive understanding of the flame retardation mechanism of polyurethane. TG-FTIR analysis was used to investigate the pyrolysis products during thermal degradation process. Fig. 8 exhibits the three-dimensional FTIR spectrograms of gaseous volatiles evolved during the whole thermal decomposition processes of WPU and PNWPU-12 in  $\text{N}_2$ . It can be intuitively seen that the absorption peaks of gaseous products for PNWPU-12 is identical to that of WPU (also see Fig. S3†). However, the absorbance intensity of PNWPU-12 volatilized products is much lower than WPU (see Fig. S4 and S5†), meaning less organic volatiles release during combustion.<sup>44</sup> The decrease of these flammable volatiles can lessen the “fuel” to feed back to flame and further result in the inhibition of smoke,<sup>45</sup> which is also verified by the reduction of THR and TSR in the cone test. More detailed information is acquired from the FTIR spectra of the sample at selected typical temperature given in Fig. 9. For WPU, a slight characteristic absorbance attributing to  $-\text{OH}$  ( $3600\text{--}3850\text{ cm}^{-1}$ , the release of water) and  $\text{CO}_2$  ( $2360\text{ cm}^{-1}$ ) are identified when the temperature rises to  $200\text{ }^\circ\text{C}$ . With increasing temperature, the nitrile compounds (HCN gases and  $-\text{NCO}$  groups,  $2265\text{ cm}^{-1}$ ) release at  $250\text{ }^\circ\text{C}$  to  $380\text{ }^\circ\text{C}$  in consequence of the decomposition of urethane groups ( $-\text{NHCOO}-$ ).<sup>46</sup> Meanwhile, some new gaseous species for hydrocarbons ( $2868\text{--}2970\text{ cm}^{-1}$ ), carbonyl compounds ( $1734\text{ cm}^{-1}$ ) and ethers ( $\text{C-O-C}$  bond,  $1112\text{ cm}^{-1}$ )<sup>47</sup> appear after  $277\text{ }^\circ\text{C}$  ( $T_{d5\%}$ ), and these FTIR signals are substantially enhanced at elevated temperature, maximizing at around

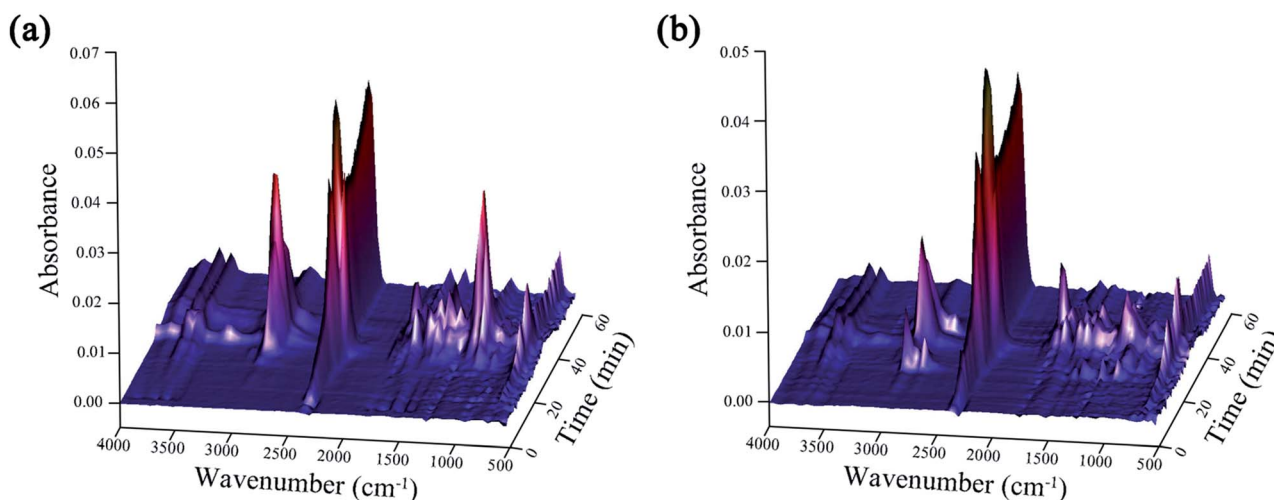


Fig. 8 Three-dimensional FTIR spectra of the gaseous volatiles evolved during the combustion of WPU (a) and PNWPU-12 (b) in  $\text{N}_2$  atmosphere.

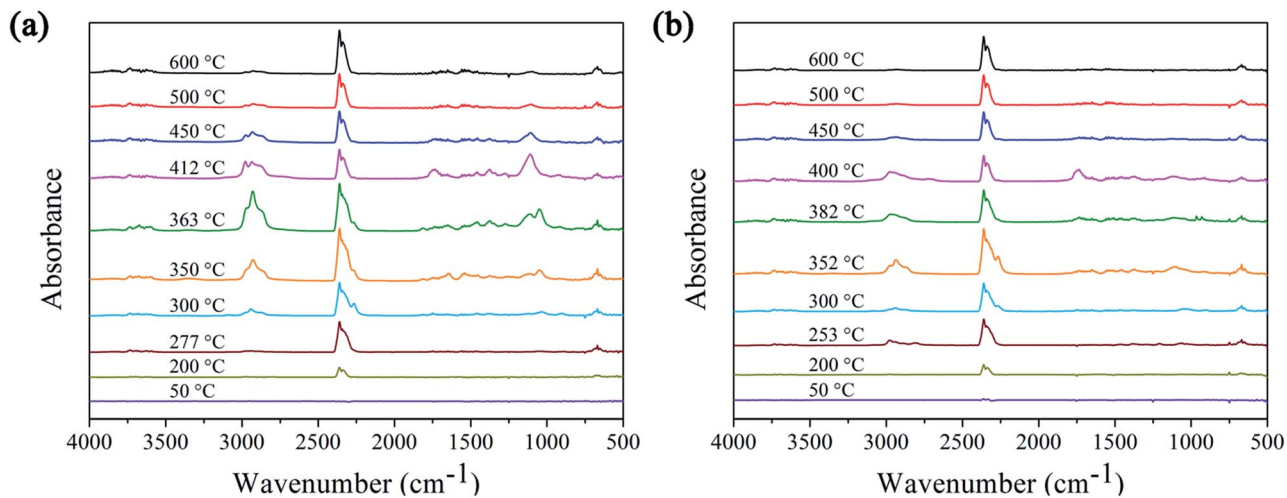


Fig. 9 FTIR spectra of pyrolysis gaseous products at typical temperatures during the thermal degradation for WPU (a) and PNWPU-12 (b).

412 °C ( $T_{\max 2}$ ) and then weakening. In the meanwhile, a small amount of nonflammable  $\text{NH}_3$  (964  $\text{cm}^{-1}$  and 930  $\text{cm}^{-1}$ ) is detected, which acts as an inert diluent in the flame zone. In contrast to WPU, PNWPU-12 begins to release pyrolysis products a slightly earlier due to the degradation of PNMPD, which coincides with the TGA results. Note that, no new absorption peaks emit in the FTIR spectra of volatile products in PNWPU-12, so it can be interpreted, again, that the fire retardancy mechanism mainly derives from the condensed phase.

Real time FTIR was employed to monitor the chemical structure changes of polyurethane in the condensed phase during thermal oxidative degradation process in  $\text{N}_2$  atmosphere. Fig. 10 depicts the RT-FTIR spectra of WPU and PNWPU-12 at different degradation temperatures. From the spectrum of WPU, the relative intensities of the characteristic absorption peaks approximately at 3379  $\text{cm}^{-1}$  (urethane N-H stretching), 1717  $\text{cm}^{-1}$  (C=O stretching vibration), 1542  $\text{cm}^{-1}$  (urethane N-H bend vibration), and 1107  $\text{cm}^{-1}$  (C-O-C)

nearly hardly change below 220 °C. As the pyrolysis temperature increases to 280 °C, all these absorptions are dimmed slightly, indicating that the polyurethane decomposes at this temperature, which is also exemplified by the TGA analysis. With further heating to 350 °C, the peaks at 3379  $\text{cm}^{-1}$ , 1717  $\text{cm}^{-1}$  and 1542  $\text{cm}^{-1}$  vanish while other absorptions decrease dramatically, thus it is unambiguously concluded that the primary decomposition, or more exactly, the scission of hard segment occurs in this corresponding stage. Meanwhile, a new absorption peak at 1626  $\text{cm}^{-1}$  is emerged, presumably representing the graphite-like structure of carbon.<sup>48</sup> Above 450 °C, almost all the characteristic peaks disappear. This observation proves the complete decomposition of the polyurethane.

As for PNWPU-12, there is no distinct difference in the absorption bands compared to WPU, apart from the peaks at 1305  $\text{cm}^{-1}$  and 1108  $\text{cm}^{-1}$  that characteristic to P=O and the overlapping of P-O-C and C-O-C, respectively. In Fig. 10b, it is

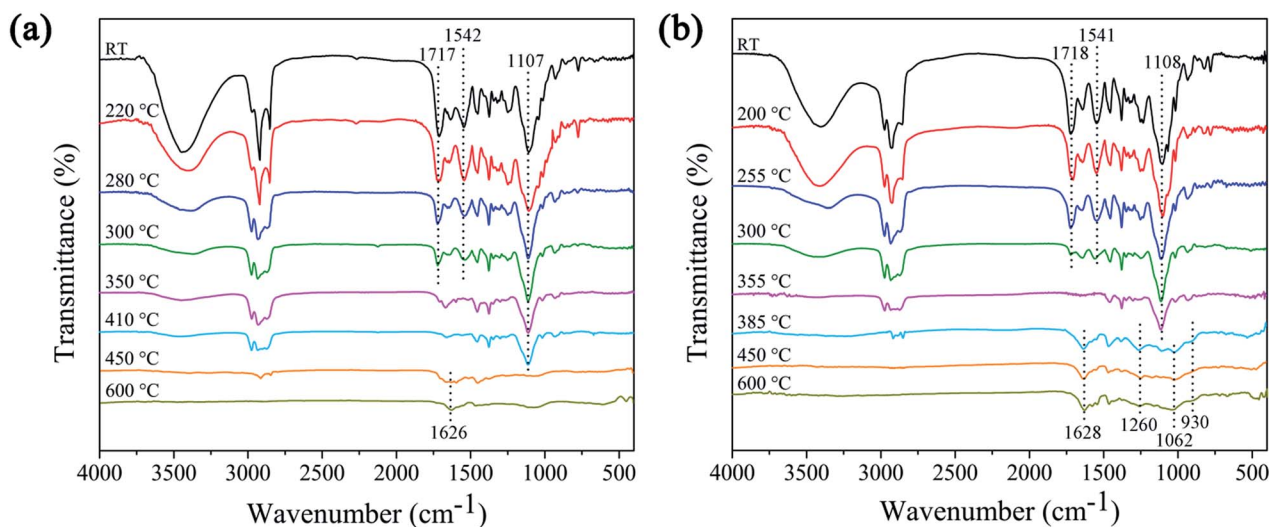
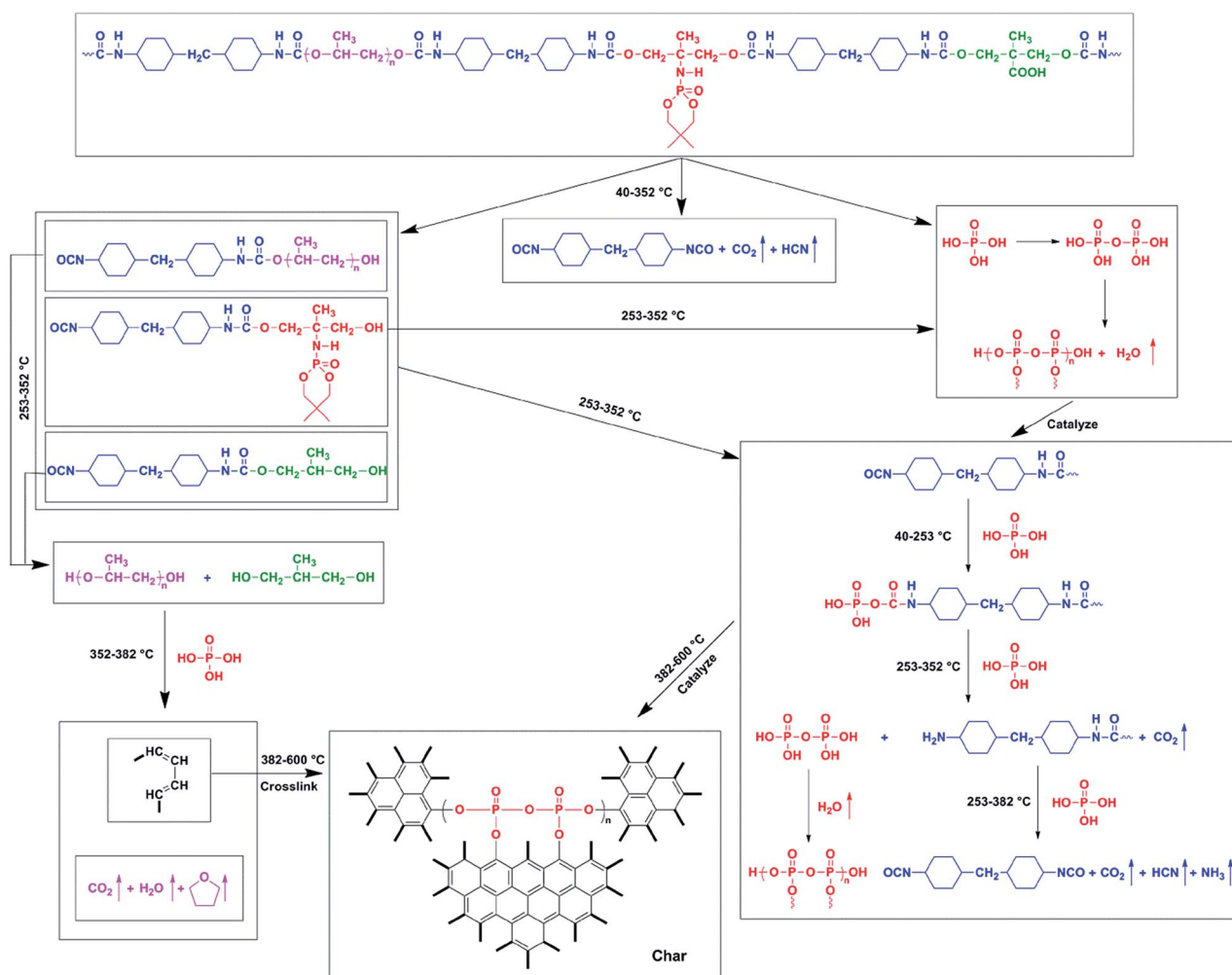


Fig. 10 RT-FTIR spectra of WPU (a) and PNWPU-12 (b) at different pyrolysis temperatures.

worth noting that the intensities of most absorption peaks become weakened gradually at 255 °C and finally disappear at 385 °C, which implies that the conjugation of PNMPD catalyzes the thermal oxidative degradation of PNWPU at lower temperature, corresponds well to the aforesaid TGA and TG-FTIR analysis. In fact, this is ascribed to the earlier cleavage of O=P-O and P-O-C linkages as disclosed by the dramatic diminution in the peaks at 1305 cm<sup>-1</sup> and 1108 cm<sup>-1</sup> before 300 °C. Compared with WPU, PNWPU-12 exhibits some new phosphorous-related characteristic absorption peaks above 355 °C. Specifically, the weak absorption appears at 1260 cm<sup>-1</sup> is assigned to the stretching mode of P=O bond. While the absorption band at 1062 cm<sup>-1</sup> (overlapping with C-O bonds) coupled with the shoulder peak around 930 cm<sup>-1</sup> in finger-print region that deriving from symmetrical and asymmetrical stretching vibrations of P-O-P structure manifests the formation of pyrophosphate in the carbon layer.<sup>49</sup> Indeed, the appearance of P-O-P structure is regarded as a testimony, demonstrating that the PNMPD plays a positive role in the condensed phase to accelerate the formation of phosphorous-containing complex-structured char residue during combustion.<sup>50</sup>

Based on the foregoing analysis and in combination with the previous literature,<sup>12,29,33,48,51</sup> a plausible thermal degradation mechanism of PNWPU is postulated and depicted schematically in Scheme 2. Firstly, the urethane groups in polyurethane main-chains and the carboxyl of DMPA degrade and release gases such as CO<sub>2</sub> and HCN at 40–253 °C. Meanwhile, the phosphorous-containing PNMPD dehydrates to form phosphoric acid. Secondly, at 253–352 °C, the phosphoric acid catalyzes the decomposition of polyurethane into polyols, isocyanates, amines, HCN and CO<sub>2</sub>. Simultaneously, phosphoric acid polymerizes to form cross-linked polyphosphoric acid and its derivatives, which serve as strong Lewis acids, and therefore catalyze the further degradation of polyols and isocyanate to form dienes at 352–382 °C with the evolution of CO<sub>2</sub>, H<sub>2</sub>O, NH<sub>3</sub>, and tetrahydrofuran. Finally, the dienes cross-link in the presence of polyphosphoric acid to form phosphorous-rich carbonaceous char with polyaromatic structures at 382–600 °C. And the thermal decomposition process of PNWPU bearing cyclic phosphoramidate lateral chains is similar to previously reported flame retardant waterborne polyurethane with phosphorus–nitrogen moieties conjugated in the main chain structures.<sup>12,48</sup>



Scheme 2 Proposed thermal degradation mechanism of PNWPU.

## 4. Conclusions

In the present work, a pendant phosphoramidate group bearing diol abbreviated as PNMPD was designed and fabricated successfully in good yields by nucleophilic substitution reaction, which was then covalently conjugated into waterborne polyurethane in the chain-extension process to enhance the fire retardancy. The as-prepared PNWPU exhibits excellent hydrolysis stability in that the hydrophobic methyl pendant groups in NPG and dioxaphosphorinane of PNMPD can well prevent water from penetrating and attacking the phosphamide moieties. Simultaneously, the PNWPU-12 exhibits a high LOI value of 27.2% and a decrease of PHRR, THR and SPR by 44.7%, 39.0% and 36.1% respectively, over WPU, illustrating the significantly improved fire resistance and sharply ameliorated smoke suppression. Moreover, TGA, TG-FTIR, RT-FTIR, SEM combined with EDX analysis further validate that the conjugation of PNMPD accelerates the degradation of PNWPU at lower temperature to promote the formation of phosphorus-rich residual chars without altering the composition of evolved products, which indicates the flame-retardant action of PNWPU is condensed phase-dominant. The rugged carbonaceous layer acts as a physical insulation barrier for underlying polyurethane to impede heat, oxygen, and flammable gaseous products from permeation to the flame during combustion.

## Acknowledgements

The authors gratefully acknowledge the financial support from the National Natural Science Foundation of China (Grant No. 21576172, 51273128 and 21206096).

## Notes and references

- 1 Y. Lu and R. C. Larock, *Biomacromolecules*, 2008, **9**, 3332–3340.
- 2 H. W. Engels, H. G. Pirkl, R. Albers, R. W. Albach, J. Krause, A. Hoffmann, H. Casselmann and J. Dormish, *Angew. Chem., Int. Ed.*, 2013, **52**, 9422–9441.
- 3 S. Bourbigot and S. Duquesne, *J. Mater. Chem.*, 2007, **17**, 2283–2300.
- 4 R. Davis, Y.-C. Li, M. Gervasio, J. Luu and Y. S. Kim, *ACS Appl. Mater. Interfaces*, 2015, **7**, 6082–6092.
- 5 S.-Y. Lu and I. Hamerton, *Prog. Polym. Sci.*, 2002, **27**, 1661–1712.
- 6 C. Hamciuc, T. Vlad-Bubulac, D. Serbezeanu, I. D. Carja, E. Hamciuc, G. Lisa and V. F. Pérez, *RSC Adv.*, 2016, **6**.
- 7 H. Zhu, Z. Peng, Y. Chen, G. Li, L. Wang, Y. Tang, R. Pang, Z. U. H. Khan and P. Wan, *RSC Adv.*, 2014, **4**, 55271–55279.
- 8 M. Thirumal, D. Khastgir, G. Nando, Y. Naik and N. K. Singha, *Polym. Degrad. Stab.*, 2010, **95**, 1138–1145.
- 9 M.-J. Chen, Z.-B. Shao, X.-L. Wang, L. Chen and Y.-Z. Wang, *Ind. Eng. Chem. Res.*, 2012, **51**, 9769–9776.
- 10 M. Neisius, S. Liang, H. Mispreuve and S. Gaan, *Ind. Eng. Chem. Res.*, 2013, **52**, 9752–9762.
- 11 Q. Tai, Y. Hu, R. K. Yuen, L. Song and H. Lu, *J. Mater. Chem.*, 2011, **21**, 6621–6627.
- 12 L. Gu and Y. Luo, *Ind. Eng. Chem. Res.*, 2015, **54**, 2431–2438.
- 13 G. Wu, J. Li, C. Chai, Z. Ge, J. Lin and Y. Luo, *RSC Adv.*, 2015, **5**, 97710–97719.
- 14 L. Gu, Z. Ge, M. Huang and Y. Luo, *J. Appl. Polym. Sci.*, 2015, **132**(3), 41288.
- 15 P. Zhang, Y. He, S. Tian, H. Fan, Y. Chen and J. Yan, *Polym. Compos.*, 2015, DOI: 10.1002/pc.23603.
- 16 M. Sato, S. Endo, Y. Araki, G. Matsuoka, S. Gyobu and H. Takeuchi, *J. Appl. Polym. Sci.*, 2000, **78**, 1134–1138.
- 17 P. Zhang, S. Tian, H. Fan, Y. Chen and J. Yan, *Prog. Org. Coat.*, 2015, **89**, 170–180.
- 18 J. L. Hodgson and M. L. Coote, *Macromolecules*, 2005, **38**, 8902–8910.
- 19 Z. Tan, C. Wu, M. Zhang, W. Lv, J. Qiu and C. Liu, *RSC Adv.*, 2014, **4**, 41705–41713.
- 20 X. Zhao, F. R. Guerrero, J. Llorca and D.-Y. Wang, *ACS Sustainable Chem. Eng.*, 2015, **4**, 202–209.
- 21 Q. Li, P. Jiang, Z. Su, P. Wei, G. Wang and X. Tang, *J. Appl. Polym. Sci.*, 2005, **96**, 854–860.
- 22 A. M. Kaushal, A. K. Chakraborti and A. K. Bansal, *Mol. Pharmaceutics*, 2008, **5**, 937–945.
- 23 N. E. Jacobsen, *NMR spectroscopy explained: simplified theory, applications and examples for organic chemistry and structural biology*, John Wiley & Sons, 2007.
- 24 P. T. Knight, K. M. Lee, H. Qin and P. T. Mather, *Biomacromolecules*, 2008, **9**, 2458–2467.
- 25 D. K. Chattopadhyay, B. Sreedhar and K. V. Raju, *Ind. Eng. Chem. Res.*, 2005, **44**, 1772–1779.
- 26 K. Kojio, M. Furukawa, Y. Nonaka and S. Nakamura, *Materials*, 2010, **3**, 5097–5110.
- 27 X. Liu, K. Xu, H. Liu, H. Cai, J. Su, Z. Fu, Y. Guo and M. Chen, *Prog. Org. Coat.*, 2011, **72**, 612–620.
- 28 M. S. Newman, *J. Am. Chem. Soc.*, 1950, **72**, 4783–4786.
- 29 D. Chattopadhyay and D. C. Webster, *Prog. Polym. Sci.*, 2009, **34**, 1068–1133.
- 30 Z. S. Petrović, Z. Zavargo, J. H. Flynn and W. J. Macknight, *J. Appl. Polym. Sci.*, 1994, **51**, 1087–1095.
- 31 J. Ding and W. Shi, *Polym. Degrad. Stab.*, 2004, **84**, 159–165.
- 32 D. Sun and Y. Yao, *Polym. Degrad. Stab.*, 2011, **96**, 1720–1724.
- 33 M.-J. Chen, C.-R. Chen, Y. Tan, J.-Q. Huang, X.-L. Wang, L. Chen and Y.-Z. Wang, *Ind. Eng. Chem. Res.*, 2014, **53**, 1160–1171.
- 34 D. Van Krevelen, *Polymer*, 1975, **16**, 615–620.
- 35 B. Schartel and T. R. Hull, *Fire Mater.*, 2007, **31**, 327–354.
- 36 H. Breulet and T. Steenhuizen, *Polym. Degrad. Stab.*, 2005, **88**, 150–158.
- 37 Y. Tan, Z.-B. Shao, X.-F. Chen, J.-W. Long, L. Chen and Y.-Z. Wang, *ACS Appl. Mater. Interfaces*, 2015, **7**, 17919–17928.
- 38 M. El Gouri, A. El Bachiri, S. E. Hegazi, M. Rafik and A. El Harfi, *Polym. Degrad. Stab.*, 2009, **94**, 2101–2106.
- 39 X. Chen, Y. Jiang and C. Jiao, *J. Hazard. Mater.*, 2014, **266**, 114–121.
- 40 U. Braun, B. Schartel, M. A. Fichera and C. Jäger, *Polym. Degrad. Stab.*, 2007, **92**, 1528–1545.
- 41 J. Feng, J. Hao, J. Du and R. Yang, *Polym. Degrad. Stab.*, 2012, **97**, 605–614.

- 42 Z. Jiang, L. Yuan, G. Liang and A. Gu, *Polym. Degrad. Stab.*, 2015, **121**, 30–41.
- 43 L. Song, Y. Hu, Y. Tang, R. Zhang, Z. Chen and W. Fan, *Polym. Degrad. Stab.*, 2005, **87**, 111–116.
- 44 B. Yu, Y. Tao, L. Liu, Y. Shi, H. Yang, G. Jie, S. Lo, Q. Tai, L. Song and Y. Hu, *RSC Adv.*, 2015, **5**, 75254–75262.
- 45 Y. Dong, Z. Gui, Y. Hu, Y. Wu and S. Jiang, *J. Hazard. Mater.*, 2012, **209**, 34–39.
- 46 H. Singh and A. Jain, *J. Appl. Polym. Sci.*, 2009, **111**, 1115–1143.
- 47 X. Wang, Y.-T. Pan, J.-T. Wan and D.-Y. Wang, *RSC Adv.*, 2014, **4**, 46164–46169.
- 48 G. Wu, J. Li and Y. Luo, *Polym. Degrad. Stab.*, 2016, **123**, 36–46.
- 49 M. Bugajny, S. Bourbigot, M. Le Bras and R. Delobel, *Polym. Int.*, 1999, **48**, 264–270.
- 50 H. Liu, X. Wang and D. Wu, *Polym. Degrad. Stab.*, 2014, **103**, 96–112.
- 51 M. M. Velencoso, M. J. Ramos, R. Klein, A. De Lucas and J. F. Rodriguez, *Polym. Degrad. Stab.*, 2014, **101**, 40–51.